COOLING LOADS REDUCTION OF OFFICE BUILDINGS INTEGRATED WITH MULTI-STORY DOUBLE-SKIN FACADES

Jae-Wan Joe[1], Won-Jun Choi[1], Seung-Chul Shin[2], and Jung-Ho Huh[1]

[1]Department of Architectural Engineering, University of Seoul, Seoul (Republic of Korea)

[2]Sustainable Building & Materials Research Center, KCC Corporation, Yongin (Republic of Korea)

Abstract

In this study, the usage of cooling energy in office buildings with multi-story double-skin façades (DSF) was analyzed. A verification model was constructed by measuring the temperature of the cavity air and the surface of office buildings where DSF had been installed, and by comparing the measurement results with the results of the EnergyPlus simulation model. The cooling loads of buildings that apply double-skin façades (DSF) and those that apply single-skin façade (SSF) were compared based on the verified model.

A case study was conducted by setting the control methods of the window between the cavity (or outdoor air) and the conditioned zone, and the activation setpoint radiation of the blind, as the variables. The amount of convection heat gain through the inside surface of inner layer, heat loss by ventilation, and the transmitted solar showed changes in each case, according to the conditions of the variables, and this had a direct effect on the cooling loads. The cooling loads of DSF and SSF seasonally changed, and the total cooling loads for DSF during the cooling season (April to October) was shown to have been reduced by 6.32% compared to the total cooling loads for SSF (Case 1 & 2). This result implies the possibility of reducing the cooling loads by using DSF in the Korean climate.

Keywords: Multi-story DSF; Validation; Cooling loads; Natural ventilation; Operation strategies; EnergyPlus

1. Introduction

The DSF system is attracting more attention as a measure for reducing energy consumption compared to the existing SSF buildings. Despite the popularity of DSF, however, there are few actual cases of buildings that have been built with DSF. Thus, there is a lack of quantitative studies on the DSF performance based on its actual construction. Especially, there is a dearth of studies concerning the multi-story double-skin façades as it is difficult to come up with experiment specimens and as there are few buildings that have been constructed using this system. Furthermore, unlike DSF's clear advantage in heating season compared to SSF, there are conflicting opinions on the advantages or disadvantages of this system in cooling season .

Gratia et al. conducted a series of simulation studies on multi-story buildings that apply multi-story double-skin facades. In two of such studies (2004, 2007), the cooling and heating loads of a building were analyzed following the infiltration level. These studies showed better results for DSF than for SSF with regard to the heating load, whereas they showed poorer results for DSF than for SSF with regard to the cooling loads. Hens et al. (2008) discovered the problems of DSF by measuring the temperature, thermal comfort, etc. of buildings that apply it, and proposed a solution, but they deduced negative results based on the thermal behavior of DSF in cooling season.

On the contrary, Hensen et al. (2002) reported the possibility of multi-story DSF reducing the cooling loads of buildings. Hamza (2008) conducted a case study on the application of DSF in the Egyptian regions, which have hot and dry climates and where natural ventilation is difficult, and proposed the possibility of DSF reducing the cooling loads. Stec et al. (2005) also devised a connective system between DSF and blind control by using an experiment specimen that applies single-story DSF, and described the advantages of DSF by analyzing the cooling and heating loads of each case.

The present series of studies based on the thermal performance of DSF showed opposing results for the variables of each study, and there is a lack of quantitative studies based on the changes in load of DSF for the study variables. Furthermore, the passive technologies of DSF should be suitable for the climate of the region where the target building is located. Thus, it is difficult for the past studies to be standardized in the Korean climate, where the seasonal changes are distinct. Accordingly, in this study, the cooling loads of buildings that do and do not apply multi-story DSF were quantitatively compared based on the model that was verified via measurement, and the possibility of DSF's reducing the cooling loads was analyzed.

2. Simulation algorithm

2.1. Airflow network method

The airflow network method (AFN) was used as the algorithm related to the flow of air current. The difference in pressure of the two continued nodes based on the Bernoulli equation is as in Eq. 1, and the added effects of wind pressure are shown in Eq. 2.

$$\Delta P = \left(P_n + \frac{\rho v_n^2}{2}\right) - \left(P_m + \frac{\rho v_m^2}{2}\right) + \rho g(z_n - z_m) \qquad \text{(Eq. 1)}$$

$$\Delta P = P_n - P_m + P_s + P_w \qquad \text{(Eq. 2)}$$

$$\Delta P_{o-i} = P_w - P_m + P_s \qquad \text{(Eq. 3)}$$

$$\Delta P_{i-i} = P_n - P_m + P_s \qquad \text{(Eq. 4)}$$

$$\dot{m} = C_d \theta \int_{z_1}^{z_2} \rho \, v(z) W \, dz \qquad \text{(Eq. 5)}$$

Each zone in AFN is expressed with a node, and the windows or cracks are expressed with linkages, which connected individual nodes. Shown in Fig. 1 is each node and linkage of DSF and SSF, where each node contains the pressure information and the linkage contains the flow rate information. The difference in pressure between the external and internal nodes is as in Eq. 3, between the internal nodes is shown in Eq. 4. The air flow of the linkages that connect each node is as in Eq. 5. A flow of one direction to three directions can be simulated on AFN, depending on the number of neutral planes on the opening.
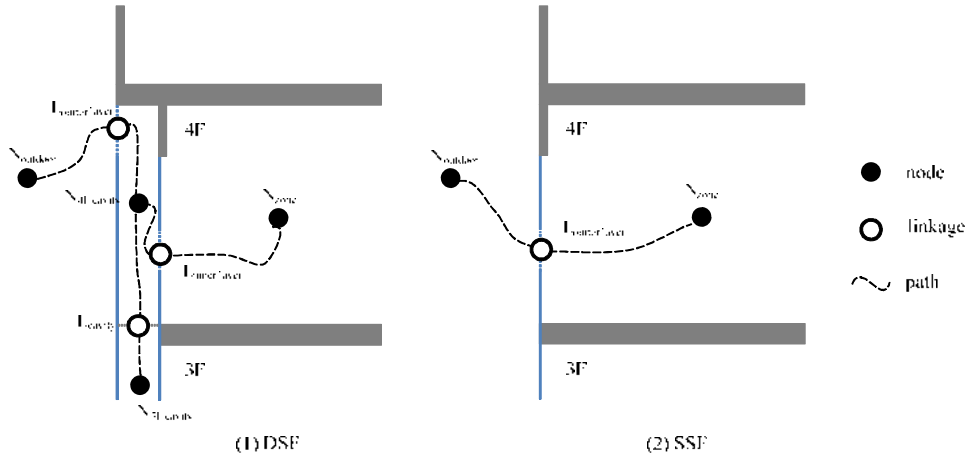

Fig. 1: Node and linkage in airflow network

2.2. Computational fluid dynamics for external air flow

Concerning the modeling of DSF in intermediate season, the external wind pressure (P_w) expressed in Eq. 3 changes according to the formation of the building and surrounding situations, and is as in Eq. 6. A CFD simulation was conducted to simulate this, and the Cp value in Eq. 6 was accordingly found.

$$P_w = C_p \frac{\rho V(z)^2}{2} \qquad \text{(Eq. 6)}$$

The algorithm used SIMPLE (Semi-implicit Method for Pressure-linked Equations) (Patankar and Spalding, 1972), and the standard k-ε model was used as the turbulence model. The computational domain and boundary conditions are as shown in Fig. 2, and the number of cells created through the grid-dependent test was approximately two million. The wind pressure coefficients entered in each surface are shown in Fig. 3.
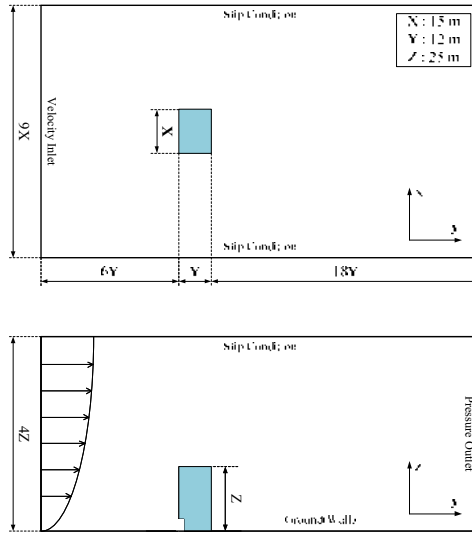
Fig. 2: Computational domain and boundary conditions

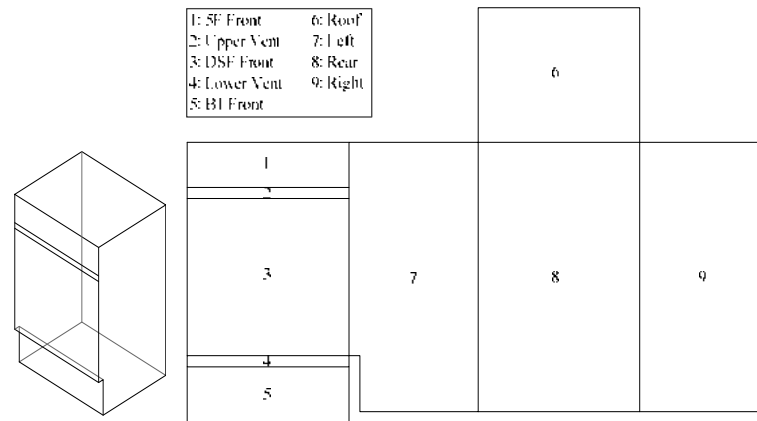|	0	30	60	90	120	150	180
Upper Vent	0.79	0.43	0.11	-0.35	-0.36	-0.24	-0.11
Lower Vent	0.31	0.07	-0.07	-0.13	-0.29	-0.35	-0.21
B1 Front	0.50	0.10	0.01	-0.15	-0.32	-0.35	-0.21
DSF Front	0.65	0.18	0.02	-0.31	-0.37	-0.28	-0.16
5F Front	0.67	0.39	0.07	-0.35	-0.35	-0.24	-0.11
Roof	-0.52	-0.34	-0.33	-0.34	-0.36	-0.38	-0.30
Left	-0.51	-0.29	-0.24	-0.16	-0.25	-0.32	-0.26
Right	-0.51	-0.02	0.24	0.31	0.20	-0.02	-0.26
Rear	-0.33	-0.25	-0.33	-0.28	0.03	0.25	0.39

Fig. 3: Wind pressure coefficient of the surfaces

3. Experiment and validation

The target building is K research laboratory building located in Yongin, Republic of Korea, which applies multi-story DSF on its southern façade. Its plan is shown in Fig. 4, and EnergyPlus 6.0 was used as the simulation tool. The experiment was conducted from February 20 to July 31, where the surface temperature (nine points on each floor) and the air temperature (four points on each floor) of the cavity were measured, while the temperature, humidity, atmospheric pressure, wind speed, wind direction and global solar radiation were simultaneously measured on the weather station located on the rooftop. The thermal and optical properties of windows used in the simulation are listed in Table 1.

The poly-crystal BIPV (Building Integrated Photovoltaic) modules were installed on 1/3 from the top of the outer layer on each floor, which blocks the solar radiation penetrating into the cavity. This façade feature was reflected in the cavity modeling on each floor by separating the zone with and without BIPV. To simulate the
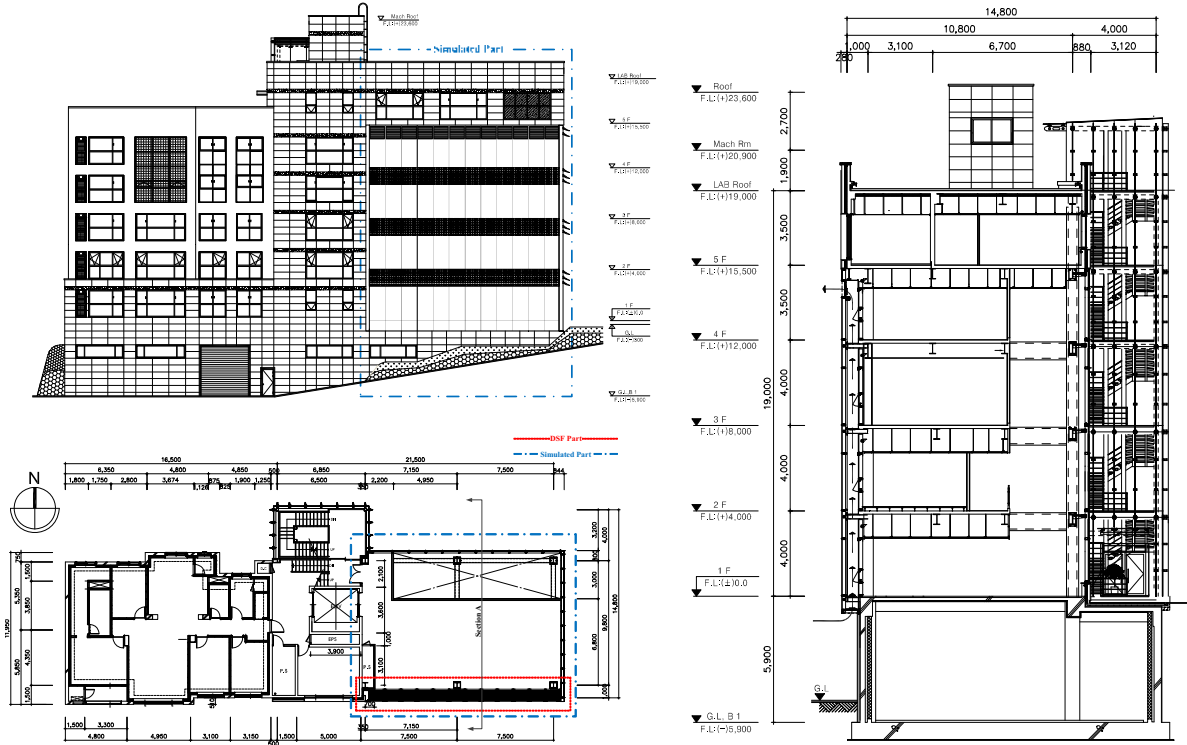
Fig. 4: Front elevation, plan and cross section of target building

airflow and stack effect between vertical zones of the cavity, virtual horizontal windows were created. These horizontal windows are linkages where uni-directional or bi-directional airflow occurs.

Shown in Fig. 5 are the verified results. The simulation temperature and averaged value of measured temperature were compared. The results displayed a correspondent rate that satisfies ±10% MBE (Mean Bias Error) and 30% Cv(RMSE) (Coefficient of Variation of the Root-Mean Squared Error), the acceptable calibration tolerances in time units, as specified by the ASHRAE Guideline 14 - Measurement of Energy and Demand Savings (2002) and Measurement and Verification Guidelines : Measurement and verification for Federal Energy Projects version 3.0 (2008). Except for the fourth floor, which was being used as an office space, all the floors were being used as operational sites or reception rooms; hence, a regular schedule did not apply. Accordingly, the inside surface of the inner layer showed results that did not quite match the results of the simulation and measurements, except for the fourth floor. Also, the measured values of the inside surface of the outer layer of the fourth floor were excluded from the graph due to data loss
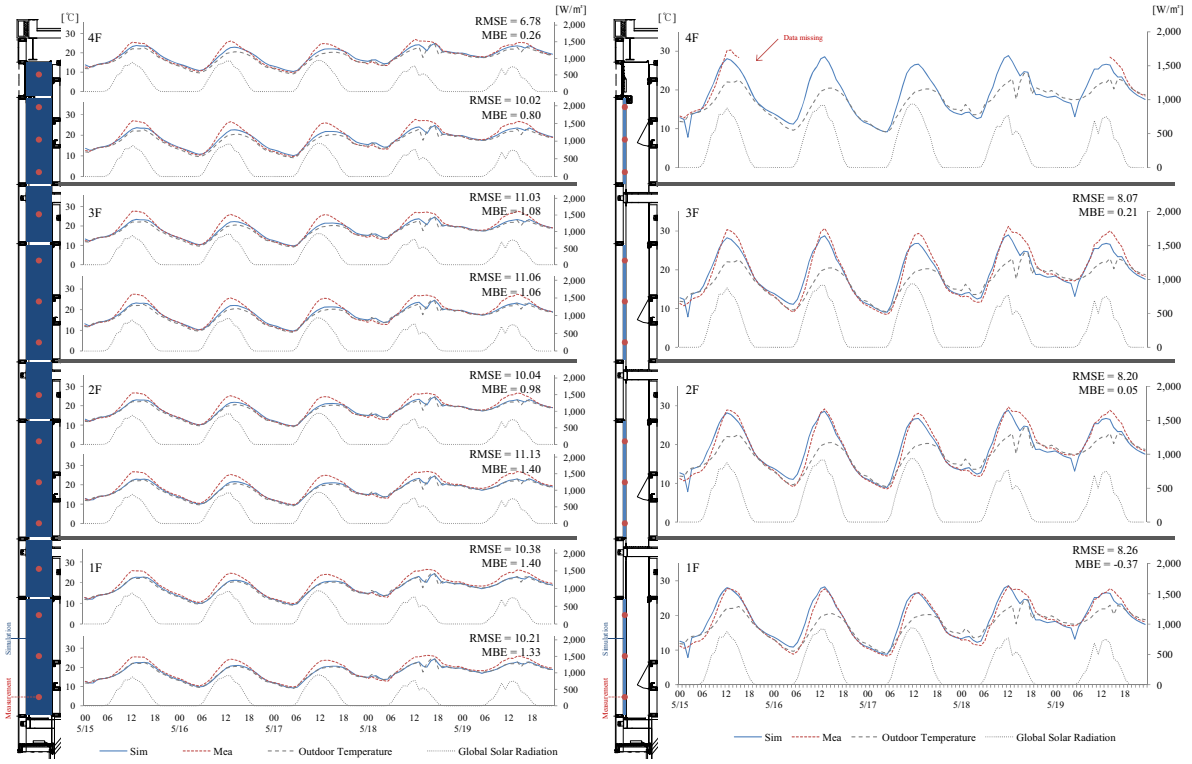
Tab. 1: Thermal and optical properties of windows

Properties		Outer layer : Single Glazing (Clr8)	Inner layer : Double Glazed low-e (Clr6 - Air12 - Lowe6)
Visible	Transmittance	0.86	0.58
	Reflectance	0.08	0.15
Solar	Transmittance	0.71	0.27
	Reflectance	0.07	0.18
U-value (W/m^2·K)		5.72	1.76
SHGC		0.77	0.38

$$RMSE = \sqrt{\frac{\sum_{i=1}^{n}(T_{sim,i}-T_{mea,i})^2}{n}}$$ (Eq. 7)
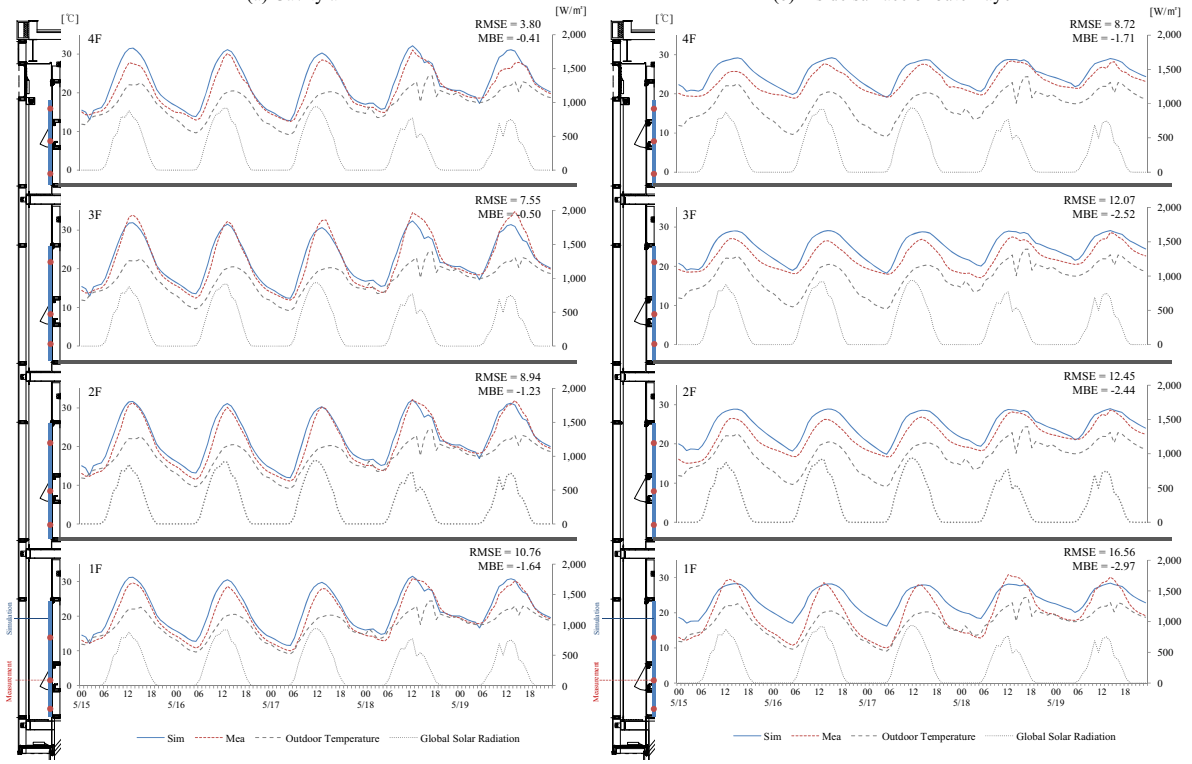
$$Cv(RMSE) = \frac{RMSE}{T_{mea,avg}} \times 100$$ (Eq. 8)

$$MBE = \frac{\sum_{i=1}^{n}(T_{sim,i}-T_{mea,i})}{n}$$ (Eq. 9)

(a) Cavity air

(b) Inside surface of outer layer

(c) Outside surface of inner layer

(d) Inside surface of inner layer

Fig. 5: Temperature validation results

4. Case study

A case study was conducted based on the verification model using Seoul weather data (Kwanho, 2010) which was generated by using ISO TRY method for thirty years. Unlike the verification model, the case study model excluded a BIPV part and was constructed to form the cavity of each floor as a single zone. The same window layers used in the verification model were applied in the DSF models (Case 2, 4, 6, 8). For the SSF models (Case 1, 3, 5, 7), however, only the double glazed low-e were used as external window layers, which correspond to the inner layer used in the DSF models. Eight cases were compared, as shown in Table 2. Cases 1

and 2 were the standard cases that were used as the comparison standards. The inner layer openings control by temperature utilizes natural-ventilation, by opening the inner layer windows if the air temperature of the cavity of each floor is lower than the air temperature of the adjacent conditioned zone. The blind was operated when the amount of solar radiation received by the external window surface was higher than the value of the blind-operation setpoint radiation. The equipment and lighting heat gain is 10 W/m^2 respectively, and one person can be accommodated for each 10 m^2 of area. The cooling setpoint temperature is 26℃, from 8 am to 6 pm. The cooling season is from April to October, and Ideal Load System of EnergyPlus, the virtual HVAC system with 100% efficiency was used.

Tab. 2: Simulation cases

Case	Facade type	Inner layer openings control	Openable windows area of the inner layer [%]	Blind-operation setpoint radiation [W/m^2]
1	SSF	temperature	13	200
2	DSF	temperature	13	200
3	SSF	*closed*	13	200
4	DSF	*closed*	13	200
5	SSF	temperature	*19.5*	200
6	DSF	temperature	*19.5*	200
7	SSF	temperature	13	*500*
8	DSF	temperature	13	*500*

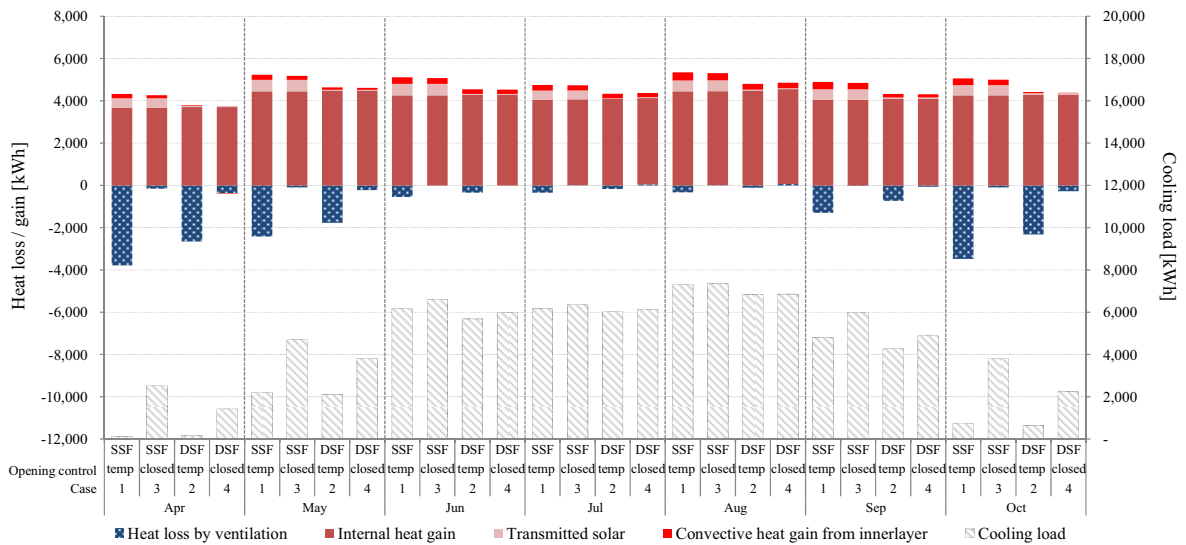*4.1 Inner layer openings control: temperature VS closed*

Fig. 6: Heat gain, loss, and cooling loads differences of cases 1, 2, 3, and 4.

In Fig. 6, unlike cases 1 and 2, which naturally ventilated the air with temperature control, cases 3 and 4 had virtually no heat loss through ventilation in all seasons. Accordingly, the cooling loads of cases 3 and 4 were dependent on the transmitted solar radiation and the convective heat gain. Case 3 gained more transmitted solar than Case 4. Thus, the cooling load in Case 3 is higher than that of Case 4 in all months.

The difference in cooling loads between cases 3 and 4 (without temperature control) and cases 1 and 2 (with temperature control) showed greater values in the intermediary periods, when natural ventilation became easier. Furthermore, DSF was slightly advantageous in all the cases, due to the difference in the transmitted solar.

In cases 1 and 2, which controlled the temperature, the heat loss through the ventilation of DSF (case 2) was smaller than that through the ventilation of SSF (case 1), but the transmitted solar radiation was also smaller. Thus, the disadvantage associated with reduction of cooling loads by ventilation in Case 2 was overcome by smaller transmitted solar.

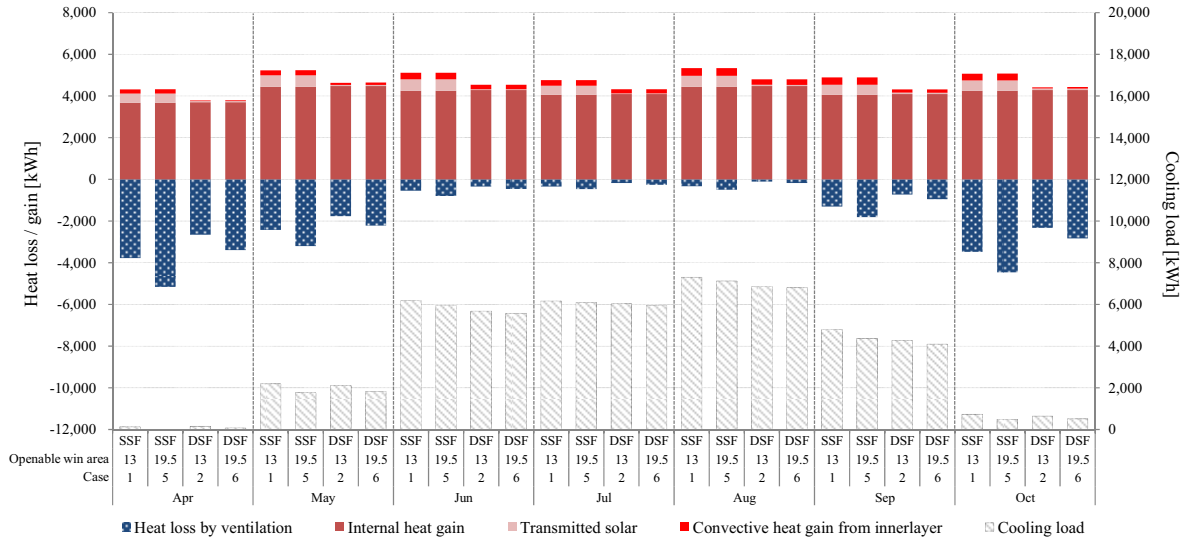## 4.2. Openable windows area of the inner layer

Fig. 7: Heat gain, loss, and cooling loads difference between cases 1, 2, 5, and 6.

In Fig. 7, the increasing flow rate through the inner layer in cases 5 and 6 increased the heat loss, and the cooling loads consequently decreased. This was clearly manifested during the intermediary periods than during summer, as natural ventilation became easier. Furthermore, DSF was slightly advantageous than SSF in all the cases, due to the difference in the transmitted solar. Comparing cases 5 and 2 during the intermediary period, the openable windows area of SSF increased, which is seen to offset the load reduction due to DSF's declined transmitted solar radiation.

Shown in Fig. 8 is heat loss by ventilation that occurred in cases 2, 4, and 6, concerning cooling on July 17. The temperature of the cavity increases in higher floors, so the volume flow through the inner layer openings decreases in higher floors. Case 4 with no ventilation, and the increased ventilation rate and heat loss of case 6 caused by increasing the openable windows area can be examined.
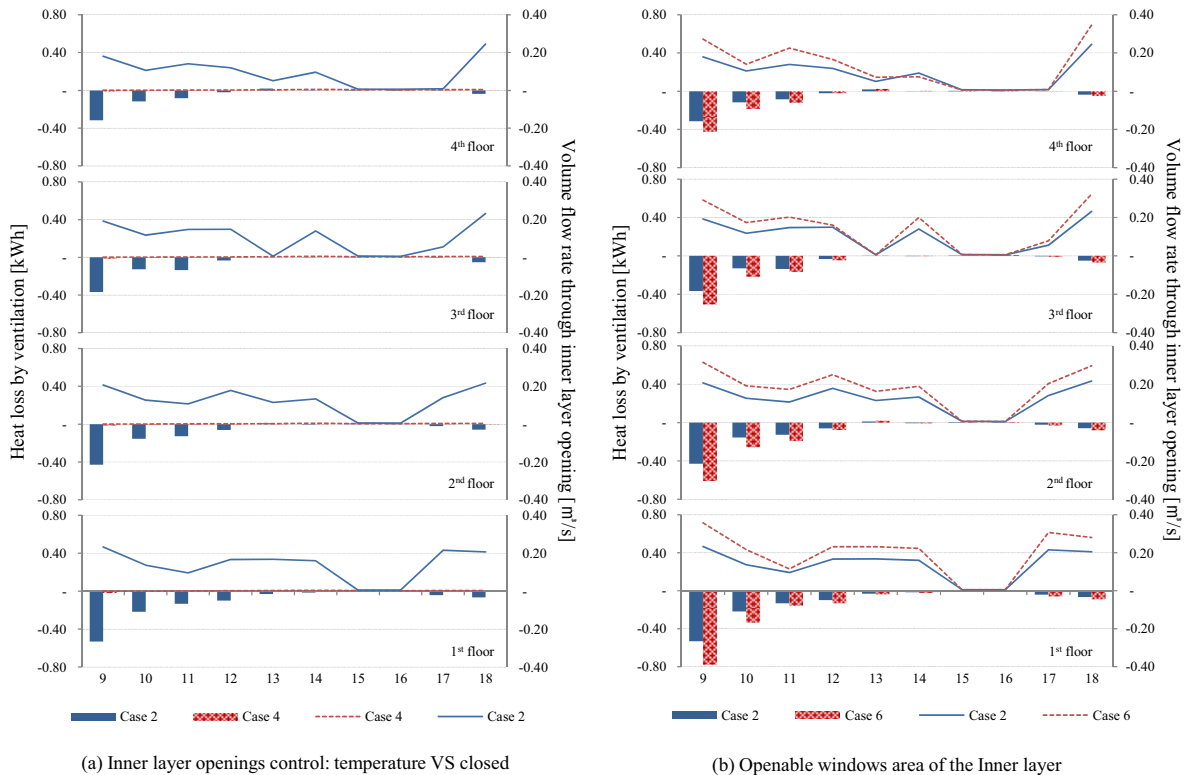

(a) Inner layer openings control: temperature VS closed

(b) Openable windows area of the Inner layer

Fig. 8: Volume flow rate through inner layer and heat loss by ventilation of case 2, 4 and 6 (17th July)

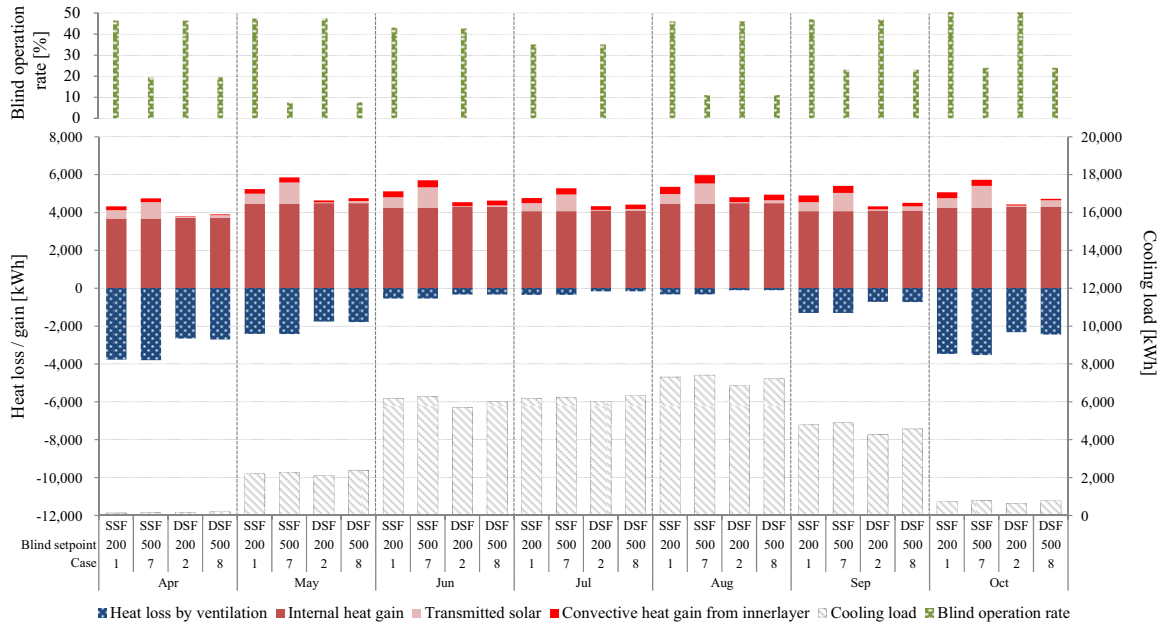## 4.3. Blind operation setpoint solar intensity

Fig. 9: Heat gain, loss, and cooling loads difference between cases 1, 2, 7, and 8.

Shown in Fig. 9 simultaneously are the heat gain, loss and load difference as well as the proportion of blind activated time during the cooling period. The blind operation time decreased as the blind operation setpoint radiation increased in cases 7 and 8. Consequently, the transmitted solar radiation increased, and the cooling loads also a small increased. This increase was relatively insignificant in DSF compared to SSF. Moreover, DSF was slightly advantageous than SSF in all the cases, due to the difference in the transmitted solar.

Shown in Fig. 10 are the transmitted solar and blind operation fraction of cases 2 and 8 during the cooling period of August 9. Bar graphs and dotted lines mean transmitted solar and blind operation fraction respectively on the left axis. Having a low blind activation time compared case 2, case 8 has a relatively high transmitted solar radiation, with the exception of midday when the amount of solar radiation received by the external windows surface reached 500.
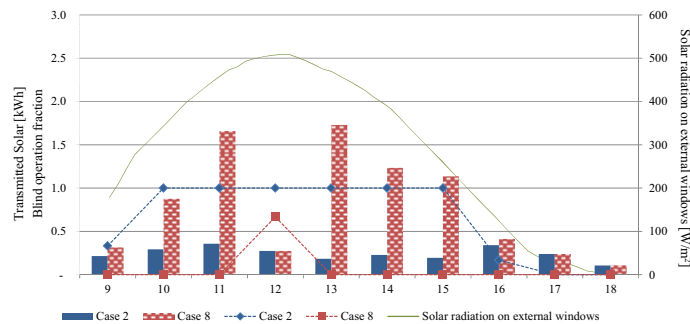

Fig. 10: Transmitted solar and blind operation fraction of Case 2 & 8 (9th August)

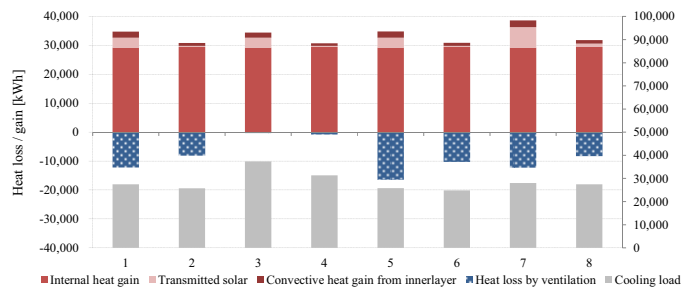## 4.4. Total cooling loads of all cases

Fig. 11: Heat loss / gain and cooling loads of all cases

Tab. 3: Cooling loads comparison of all cases

Case	1	2	3	4	5	6	7	8
Cooling loads [kWh]	27,47	25,74	37,33	31,34	25,77	24,80	27,99	27,46
Cooling loads difference [%]	compared to 1,2		35.88	21.77	-6.18	-3.63	1.89	6.69
	compared to 1	-6.32	compared to 3	-16.05	compared to 5	-3.77	compared to 7	-1.9
	compared to 1		-	14.08	-	-9.72	-	-0.05

Fig. 11 shows the total heat loss and gain, and the cooling loads of each case. Table 3 displays the comparison of the total cooling loads of each case from April to October. Controlling the inner layer openings with temperature, and having a greater openable windows area of the inner layer and lower blind operation setpoint solar intensity displayed good results on the cooling loads. Furthermore, DSF and SSF have been compared on all control methods to display individual advantages at 6.32, 16.05, 3.77 and 1.90 %. These advantages are judged to manifest on the cooling loads, as the transmitted solar radiation decreases, even with a decreased rate of ventilation on the double-skin façades.

5. Conclusions

The air temperature of the cavity of office buildings installed with DSF has been measured and investigated by comparing with a simulation model. A case study was conducted by setting the operation strategies and openable windows area of the inner layer, and blind operation setpoint radiation based on the verification model. The results are as follows.

DSF is disadvantageous concerning the rate of ventilation in comparison to SSF, with the exception of high-rise buildings whose external surfaces are exposed to strong wind pressure. However, it is advantageous on the cooling loads, as the obtainment of heat by transmitted solar radiation is low. Also, DSF is advantageous for convective heat gain on the inner layer concerning the cooling loads, but did not show great effect. Ultimately DSF showed to be advantageous than SSF by 1.9 ~ 16.5% in all cases. Furthermore, both SSF and DSF showed advantage on the cooling loads with greater effect in blocking the transmitted solar radiation by decreasing the blind operation setpoint radiation and in increasing the ventilation rate by utilizing temperature control of the larger openable windows area in the inner layer.

However, the blocking of solar radiation with blinds refers to the increase in the use of lighting energy during dimming control, which has not been included in this paper. Furthermore, all results of this study are restricted to the investigated building in the Korean climate.

6. Nomenclature

ΔP : pressure difference between nodes n and m [Pa]

$P_{n,m}$: pressure at nodes n and m [Pa]

ρ : air density [kg/m^3]

$v_{n,m}$: air velocity at nodes n and m [m/s]

g : acceleration due to gravity [m/s^2]

$z_{n,m}$: height at nodes n and m [m]

P_s : pressure difference due to the difference of density and height [Pa]

P_w : pressure difference due to the wind [Pa]

P_{o-i} : pressure difference between internal and external node [Pa]

P_{i-i} : pressure difference between internal nodes [Pa]

$\dot{m}$: mass flow rate [kg /s]

C_d : discharge coefficient

$z_{1,2}$: top or bottom elevation of opening area [m]

$v(z)$: air velocity at elevation z [m/s]

W : opening width [m]

C_p : $wind$ $pressure$ coefficient

T_{sim} : simulated temperature [ºC]

T_{mea} : measured temperature [ºC]

$T_{mea,avg}$: average of measured temperature [ºC]

n : a number of data

7. Reference

ASHRAE, 2002, ASHRAE Guideline 14-Measurement of Energy and Demand Savings, American Society of Heating, Refrigerating and Air-Conditioning Engineers.

EnergyPlus Engineeering Document, 2010, in Version 6.0, U.S. Department of Energy.

Gratia, E., De Herde, A., 2004, Optimal operation of a south double-skin facade, Energy and Buildings, vol. 36, pp.41-60.

Gratia, E., De Herde, A., 2007, Are energy consumptions decreased with the addition of a double-skin?, Energy and Buildings, vol. 39, pp.605-619.

Hensen, J.L.M., et al., 2002, Modeling and simulation of a double-skin façades system, ASHRAE transactions, vol. 108, part2, pp.1251-1259.

Hamza, N., 2008, Double versus single skin Façades in hot arid areas, Energy and Buildings, vol. 40, pp.240-248.

Hens, H., et al., 2008, Multiple-skin facades: high tech blessing or not?, Proceedings of the 8th Symposium on Building Physics in the Nordic Countries, edition:8, pp.1-8.

International Standard ISO 15972-4, 2005, Hygrothermal performance of buildings-Calculation and presentation of climatic data-Part 4: Hourly data for assessing the annual energy use for heating and cooling.

Kwanho, L., et al., 2010, Generation of typical weather data using the ISO Test Reference Year (TRY) method for major cities of South Korea, Building and Environment, vol. 45, pp.956–963.

Lixing, G., 2006, Airflow network modeling in EnergyPlus, Proceeding: Building Simulation 2007, pp.964-971.

Patankar, S.V., Spalding, D.B., 1972, A calculation procedure for heat, mass and momentum transfer in three-dimensional parabolic flows, Int. J. Heat Mass Transfer, vol. 15, p.1787.

Stec, W. J., 2005, Symbiosis of the double skin façade with the HVAC system, Energy and Buildings, vol. 37, pp.461-469.

U.S. DOE Federal Energy Management Program, 2008, Measurement and Verification Guidelines : Measurement and Verification for Federal Energy Projects Version 3.0, U.S. Department of Energy.

Walton, G.N., 1989, AIRNET – A computer program for building airflow network modelling, National Institute of Standards and Technology, NISTIR 89-4072, Gaithersburg, Maryland.

Choi, W.J., 2011, Operation and control strategies for the multi-story Double-skin Facades, M.Sc. thesis, Department of Architectural Engineering, University of Seoul, Korea.